Università degli studi di Udine

Experimental evaluation of CO2/R-152a mixtures in a refrigeration plant with and without IHX

(Article begins on next page)

22 December 2024

Experimental evaluation of CO₂/R-152a mixtures in a refrigeration plant with and without IHX

Sicco E.[b], Martínez-Ángeles M.[a], Toffoletti G.[b], Nebot-Andrés L.[a],[*],[α]
Sánchez D.[a], Cabello R.[a], Cortella G. [β],[b], Llopis R.[a],[α]

[a] Thermal Engineering Group, Mechanical Engineering and Construction Department,
Jaume I University, Spain

[b] Dipartimento Politecnico di Ingegneria e Architettura, Università degli Studi di Udine, Italy

*Corresponding author: lnebot@uji.es, +34 964 718133

[α] IIF Member, Commission B2

[β] IIF Member, Commission D1

Abstract

In recent years, CO₂-based mixtures have been considered as a way to improve the performance of refrigerating plants using pure CO₂ as refrigerant. Combining CO₂ with a fluid with higher critical temperature generates a blend which allows to run a refrigeration plant in subcritical conditions at higher heat rejection temperature when compared to pure carbon dioxide, and consequently reach higher COP. This work evaluates from an experimental point of view two CO₂/R-152a mixtures, ([90/10%] and [95/5%]), used as refrigerants in a single-stage refrigeration plant with and without internal heat exchanger, and compares the results to those obtained using pure CO₂. The work analyses the main energy parameters of the plant for secondary fluid inlet temperature of 2.5ºC at the evaporator, and in the range from 20 ºC to 40 ºC with 5ºC step at the condenser/gas-cooler. The use of such mixtures, compared to the use of pure CO₂, allowed to obtain a higher COP in the base cycle for heat rejection temperature above 25ºC, reaching the largest increment at the highest temperature while, when working with IHX cycle, no improvements in the COP were measured.

Keywords

CO₂; R-152a; internal heat exchanger; refrigerant mixtures

Nomenclature

BP	refers to back-pressure valve
COP	coefficient of performance
C_p	specific heat capacity, kJ·kg^{-1}·K^{-1}
EXV	expansion valve
h	specific enthalpy, kJ·kg^{-1}
I	uncertainty
IHX	internal heat exchanger
$\dot{m}$	mass flow rate, kg·s^{-1}
M	mass

p	pressure, bar
Pc	power consumption, W
p_C	critical pressure, bar
PC	refers to parallel compression layout
$\dot{Q}_o$	cooling capacity, W
SH	degree of superheat in the evaporator, K
t	temperature, ºC
t_C	critical temperature, ºC
$\dot{V}$	volumetric flow, $m^3 \cdot h^{-1}$
VCC	volumetric cooling capacity, $kJ \cdot m^{-3}$
x	quality or vapour title
Z	composition

Greek symbols

| ε | thermal effectiveness |
| ρ | density, $kg \cdot m^{-3}$ |

Subscripts

dis	compressor discharge
g	refers to propylene glycol/water mixture
gc	refers to gas-cooler
in	inlet
k	condenser
l	saturated liquid / liquid side in the IHX
main	refers to the main compressor
o	refers to evaporator
out	outlet
ref	refrigerant
sub	subcooling
sf	secondary fluid
v	saturated vapour / vapour side in the IHX
w	refers to water

1. Introduction

The 2nd F-Gas Regulation (European Commission, 2014) supposed the start of phasing-out high-GWP refrigerants in medium and large refrigeration systems, especially in supermarket centralized refrigeration. This regulation is now under modification, but its approval is still pending. However, from the proposal draft, it will accelerate the phase-down of artificial refrigerants in Europe favouring natural substances or very low GWP fluids (European Comission, 2023). From 2014 on, CO_2-based refrigeration supermarkets proliferated in Europe, reaching more than 57000 units in 2022 according to ATMOsphere (2022). Among them, 87.7% CO_2-stores implement medium or large-sized architectures (cooling capacity >40kW), 3.5% are industrial systems and only 8.8% are systems for low-sized capacities, which are usually known as condensing units. The high percentage of large CO_2 systems is explained with economic reasons, since they allow higher investment rate, so they can rely on advanced refrigeration architectures such as parallel compression (Karampour and Sawalha, 2018; Nebot-Andrés et al., 2021a), ejectors (Gullo et al., 2018; Purohit et al., 2018), mechanical subcooling systems (Bush et al., 2017; Catalán-Gil et al., 2019; Nebot-Andrés et al., 2022) flooded evaporator (Lata and Gupta, 2020; Söylemez et al., 2022), among others. However, the investment in high-efficiency CO_2 cycles for low-capacity systems is not usually profitable, so they usually still rely on condensing units operating with HFC or other synthetic fluids such as the family of HFOs or some HCFOs (R-1233zd(E)).

During the last years, there has been a rising interest to extend the use of CO_2 to low-capacity systems by using refrigerant blending. From a theoretical perspective, Kumar and Kumar (2019) investigated the use of R-290 as doping agent of CO_2 with 15% of mass proportion. They reported that the use of that blend in the refrigeration cycle was able to reduce the optimum high pressure allowing subcritical operation, but they did not find COP improvement. Zhao et al. (2022) considered CO_2 blending with butane, isobutane and two HFOs for the application as refrigerants in single and two-stage cycles with IHX for LT applications. The use of all the evaluated mixtures offered COP increments in relation to CO_2. Xie et al. (2022) extended the analysis considering CO_2/R-152a and CO_2/R-161 blends used as working fluids in single-stage cycles. At the evaluated conditions, they predicted 26% increase of COP in relation to the use of pure CO_2. Vaccaro et al. (2022) enlarged the analysis to blends composed by CO_2 and three HCs (R-600a, R-600 and R-290), two HFOs (R-1234ze(E) and R-1234ze(Z)) and one HCFO (R-1233zd(E)). They concluded that at -15ºC of evaporation and 40ºC at the exit of the gas-cooler the use of blends CO_2/R-1234yf and CO_2/R-290as refrigerants gave the best results in terms of energy efficiency, offering COP increments up to 12.8% and 7.9% when compared to the use of pure CO_2, respectively using a single-stage configuration and one with IHX. And recently, Martínez-Angeles et al. (2023) evaluated CO_2-doping with R-152a, R-1234yf, R-1234ze(E) and R-1233zd(E) considering the single-stage cycle with IHX and the parallel compression. They predicted maximum increments up to 5.8% for the IHX layout and 10.0% for the PC cycle.

Experimental validation of the theoretical hypothesis is scarce, but Tobaly P. et al. (2018) were able to measure 19.7% COP increment in relation to CO_2 using the mixture CO_2/R-290 [90/10%] as refrigerant at air-conditioning conditions with a single-stage test rig with IHX and scroll compressor. Later, Yu et al. (2018) extended the analysis of CO_2/R-290 mixtures as working fluid in MAC systems measuring 22% COP increments. Sánchez et al. (2019) (2020) evaluated R-290, R-1270 and R-32 as doping agents of CO_2 in order to create fluids that were used as refrigerants in a beverage cooler for positive temperature applications. In this case, under fixed climatic chamber conditions, they measured energy consumption reductions in relation to pure-CO_2 up to 17.2% at an environment temperature of 25ºC and up to 12.2% at 30ºC. Recently, Sánchez et al. (2023b) (2023a) analysed experimentally CO_2-based mixtures in transcritical

cycles and reported maximum COP enhancements of 21.4% and 8.7% for CO_2/R-32 and CO_2/R-1270 respectively. These works confirm that it is possible to enhance the performance of basic cycles which use CO_2 as working fluid by using, instead, a blend made by doping the pure CO_2 with a small quantity of another fluid. However, the existing works are focused on air-conditioning systems or small stand-alone refrigeration systems and no works have been found in relation to condensing unit applicable to small-sized refrigeration applications.

Therefore, the present work aims to contribute to the CO_2 refrigerant blends study by providing the results of the experimental evaluation of the use of two CO_2/R-152a blends ([90/10%] and [95/5%]) as refrigerants in a single-stage test rig for commercial purposes at MT level with two refrigeration architectures, the base configuration and the one with IHX. The work, which provides validation of the heat transfer fluids in condenser/gas-cooler and evaporator, confirms that the COP of the system can be enhanced using the tested blends as refrigerants instead of pure CO_2; however, the measured increments are lower than the ones predicted theoretically.

2. Materials and methods

2.1. Experimental test plant

The experimental tests were realized with a water-to-water single-stage transcritical refrigeration plant with a double-stage expansion system, whose scheme is detailed in Figure 1. It is driven by a Dorin CD380H semi hermetic compressor with a displacement of 3.0 $m^3 \cdot h^{-1}$ at nominal speed. Evaporator and condenser/gas-cooler are brazed plate counter-current heat exchangers with exchange surface area of 4.794 m^2 and 1.224 m^2, respectively. It incorporates a single-pass double pipe IHX arranged in counterflow with a heat transfer surface area of 0.1194 m^2 which can be included or not in the cycle by opening or closing manual ball valves. Plant is regulated using two electronic expansion valves, a Carel E2V18 for the back-pressure valve and a Carel E2V14 for controlling the evaporating process. The first regulates the heat rejection pressure using a custom-made PID controller and the second operates as a thermostatic valve with external equalization. The coefficients of the expansion valve of the evaporator are adjusted for the operation of each refrigerant.
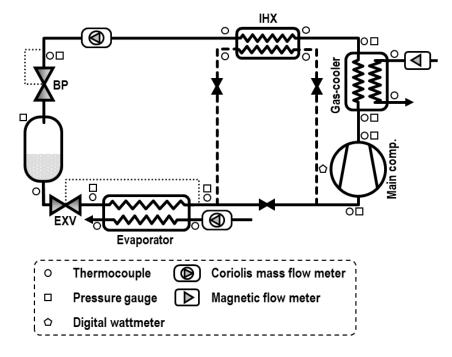
Figure 1. Schematic diagram of the experimental test bench

The plant is fully instrumented to determine its energy performance (see sensor allocation in Figure 1). It incorporates 16 T-type thermocouples (immersion thermocouples for the condenser/gas-cooler exit and evaporator, the rest are placed over the pipe surface), 4 high pressure gauges, 1 medium pressure gauge and 3 low pressure gauges. Refrigerant mass flow rate is measured with a Coriolis mass flow meter at the high-pressure line prior to the back-pressure valve, volumetric water flow to the gas-cooler is measured using a volumetric flow meter and the water-propylene glycol mixture (60/40% by volume) mass flow is measured using another Coriolis mass flow meter. The compressor electric power is measured using a digital wattmeter. The calibration range and measurement error of the instrumentation are detailed in Table 1.

Table 1. Calibration range and measurement error of instrumentation

2.2. Selected refrigerant mixtures and preparation

The theoretical simulations of Xie et al. (2022) and Martínez-Ángeles et al. (2023) concluded that CO_2/R-152a mixtures could improve the performance of transcritical cycles in relation to pure CO_2. In addition, the interaction coefficients of the equations of state of CO_2/R-152a mixtures were fitted from experimental data by Bell and Lemmon (2016); thus Refprop v.10 (Lemmon E. W. et al., 2018), which is the software used to predict the thermophysical properties of the fluids, presents validated mixing rules. As R-152a provided, from a theoretical point of view, one of the highest energy improvements and its mixing rules with CO_2 were confident (Martínez-Ángeles et al., 2023), authors selected the fluid R-152a as doping agent of CO_2 to perform the experimentation covered by the present work. Additionally, authors tested R-1233zd(E) in the plant, but due to the absence of confident mixing rules validation of energy measurements was not possible and they are not included in this work.

R-152a is a refrigerant with higher critical temperature and lower critical pressure than CO_2. Theoretical studies indicate that the use of CO_2/R-152a mixtures as refrigerants instead of pure CO_2 could be a way to enhance the COP of a

refrigeration cycle. The largest COP enhancements are predicted with R-152a mass fraction between 5 % and 10%, its optimum composition depending on the heat rejection temperature. CO_2 and CO_2/R-152a mixtures with 5 and 10% mass percentage of R-152a are evaluated. The upper limit of 10% is fixed at that percentage in order not to cause large VCC differences in comparison with the compressor working with pure CO_2. Working with a VCC distant from the compressor design one would induce malfunctions in the compressor and consequently in the cycle. On the other hand, composition of 5% of R-152a was decided based on the previous study since the optimum composition of the additive is located around 5% depending on heat rejection temperatures. This work does not cover the search for the optimum proportion of R-152a, since this investigation must be focused on a given application, which is out of the purpose of the work.

The pressure enthalpy diagrams of the three fluids are depicted in Figure 2 and some selected thermophysical properties are presented in Table 2. The addition of such a proportion of R-152a to CO_2 induces small changes in the thermophysical properties, as seen in Figure 2. In relation to the benefits, the critical temperature increases 10.6 K for 10% R-152a addition, thus the region at which the plant operates in transcritical conditions is reduced. The working pressures at the low- and high-pressure sides decrease (for 10% addition: 3.6 bar at -10ºC and 10.7 at 30ºC) and the latent heat of phase change widens (for 10% addition: 10.0% more at -10ºC and 150.5% more at 30ºC). However, the addition of R-152a introduces two important drawbacks: R-152a has high specific volume, therefore the mixtures increment the specific volume (for 10% addition: 86.4% more) and it could reduce the volumetric cooling capacity (VCC) of the plant; also, since R-152a has a different normal boiling point, it introduces a temperature glide in the phase change temperatures (for 10% addition: 13.3K at -10ºC and 6.6K at 30ºC), which reduces the thermal effectiveness of evaporator and condenser (when operating in subcritical conditions). Nonetheless, the temperature glide in the gas-cooler could be beneficial. As mentioned, there are drawbacks and benefits of doping CO_2 with R-152a, however, they have not been evaluated using an experimental approach yet.
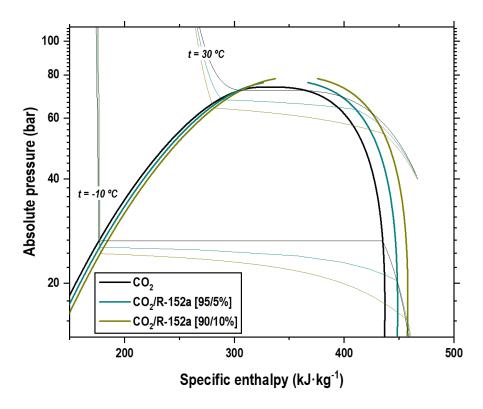
Figure 2. Pressure-enthalpy diagram of the three tested fluids

In relation to the mixture preparation, the plant was charged in all the cases using 12 kg of total mass of mixture, guaranteeing that at the exit of the vessel the refrigerant was in saturated liquid conditions. It was verified visually through a sight glass in the vessel. Fluids used to prepare the mixtures were certified 99.9% purity gases. To avoid errors in the mixture preparation, first a vacuum procedure was made in the plant; then, the corresponding quantity of R-152a was introduced in the plant (1.2 kg of R-152a for 10%); and finally, the plant was filled with CO_2 until 12 kg (10.8 kg of CO_2 for 10%). The charging procedure was controlled using a certified mass balance with a measurement error of 5 g. The uncertainty of the refrigerant compositions was for 5% of R-152a [94.96/5.04%] and [95.04/4.96%], and for 10% of R-152a [89.96/10.04%] and [90.04/9.96%].

2.3. Experimental methodology

Fluids comparison was made setting the plant to the same inlet conditions of secondary fluids. In the evaporator. The secondary fluid used was a water/propylene glycol mixture (60/40% by volume), with a constant volumetric flow of 0.7 $m^3 \cdot h^{-1}$ and a constant inlet temperature of 2.5 °C, while the secondary fluid used in the condenser/gas-cooler was water, with a constant volumetric flow of 1.17 $m^3 \cdot h^{-1}$. The plant was run with the compressor at the nominal speed (50 Hz) and was tested at water inlet temperatures to the condenser/gas-cooler from 20 °C to 40 °C with 5°C steps for the base configuration and up to 35 °C for the IHX to keep the discharge temperature below 140 °C. Unfortunately, a couple of tests with the mixture CO_2/R-152a [95/5%] at 20 °C could not be performed due to limitations of the heat dissipation system which could not reject all the heat from the gas-cooler/condenser at lower temperatures (20°C). Thus, it was not possible to achieve the desired water inlet temperature and perform the test.

For each test condition, the high-pressure of the plant was optimized to reach the maximum COP value (Nebot-Andrés et al. (2021b)).

3. Results

This section presents and discusses the experimental results obtained heat rejection temperatures ranged from 20ºC to 40ºC. This campaign contents result Subsection 3.1 focuses on the evaluation of the plant without IHX (i.e. "base" configuration), subsection 3.2 with IHX, and subsection 3.3 synthetizes the energy improvements obtained by the use of CO_2-doped mixtures.

3.1. Base configuration

Cooling capacity is calculated as the product of refrigerant mass flow rate in the evaporator and the enthalpy difference between the outlet and the inlet of the evaporator. Nonetheless, inlet enthalpy of the evaporator is calculated as the enthalpy at the Back Pressure valve, considering an isenthalpic expansion and neglecting heat loss:

$$\dot{Q}_O = \dot{m}_{ref} \cdot (h_{o,out} - h_{bp,in}) \tag{1}$$

The value of cooling capacity is expressed by, taking into account the uncertainty:

$$\dot{Q}_o = \dot{Q}_o \pm I_{\dot{Q}_o} \tag{2}$$

Where the uncertainty is evaluated as Eq. (3) and detailed in Appendix 1

$$I_{\dot{Q}_o} = \sqrt{\left((h_{o,out} - h_{bp,in}) \cdot \varepsilon_{\dot{m}}\right)^2 + \left(\dot{m}_{ref} \cdot I_{h_{o,out}}\right)^2 + \left(\dot{m}_{ref} \cdot I_{h_{bp,in}}\right)^2} \tag{3}$$

Apart from the previous equation, cooling capacity can also be calculated through the secondary fluid performing a heat balance as outlined in Eq. (4). Both calculated cooling capacities are compared, to validate the obtained results (Table 3 and Table 4).

$$\dot{Q}_{O,sf} = \dot{V}_g \cdot \rho \cdot \bar{c}_p \cdot (t_{g,in} - t_{g,out}) \tag{4}$$

The COP of the system is the ratio between the cooling capacity and the electrical power of the compressor, as exposed in Eq. (5).

$$COP = \frac{\dot{Q}_O}{P_C} \tag{5}$$

Its uncertainty is evaluated with:

$$I_{COP} = \sqrt{\left(\frac{1}{P_C} \cdot I_{\dot{Q}_o}\right)^2 + \left(\frac{-\dot{Q}_o}{P_C^2} \cdot \varepsilon_{P_C}\right)^2} \tag{6}$$

In the condenser/gas-cooler, the heat transfer rate has been calculated both on the refrigerant side as shown in Eq. (7) and on the water secondary loop side, using Eq.(8).

$$\dot{Q}_{gc} = \dot{m}_{ref} \cdot (h_{gc,in} - h_{gc,out}) \tag{7}$$

$$\dot{Q}_{gc,sf} = \dot{m}_w \cdot \bar{c}_p \cdot (t_{w,out} - t_{w,in}) \tag{8}$$

Figure 3 shows the (p-h) diagrams of the base cycle configuration obtained at the highest COP conditions for each evaluated refrigerant, represented for a water inlet temperature to the gas cooler of 30°C. In the three diagrams it can be observed that the critical temperature of the fluid increases with the addition of R-152a. While the cycle that uses pure CO_2 as refrigerant works in supercritical conditions, the cycles which use the mixtures as working fluid work in the critical zone or even subcritical conditions for the blend with 10% of R-152a. This is due to the fact that the critical pressure of the mixtures is higher if compared to the one of the pure CO_2, and the optimum working pressure is reduced when the mixtures are used instead of the CO_2. Therefore, the use of mixtures gives place to subcooled liquid at the exit of the condenser.
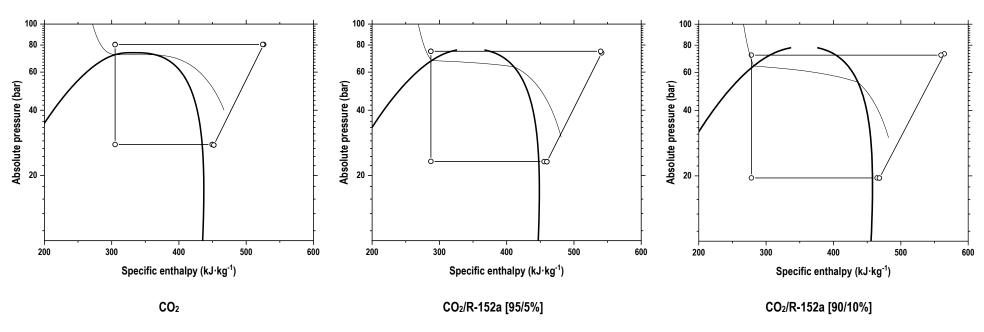
Figure 3. Refrigerating cycles sketched in the (p-h) diagrams of CO_2 and mixtures for base configuration at $t_{w,in}$=30 ºC, at optimum conditions

3.1.1 COP

For the base cycle, the measured COP values and their uncertainties for each condition using the three tested fluids are displayed in Figure 4. As it can be seen, there are different trends that must be noted. With the use of mixture CO_2/R-152a [95/5%] better COP values are obtained, when compared to the COP measured using pure CO_2, which is the reference for this work. The use of the blend CO_2/R-152a [90/10%] shows a different behaviour, as COP values calculated for temperatures below 25ºC are lower than the ones obtained with the use of pure CO_2. However, above the mentioned temperature the COP values obtained using this mixture are higher than the ones given by the use of pure CO_2 and at the highest temperature its performance overcomes even the one given by using CO_2/R-152a [95/5%]. All the COP values and their uncertainties are presented in Table 3.
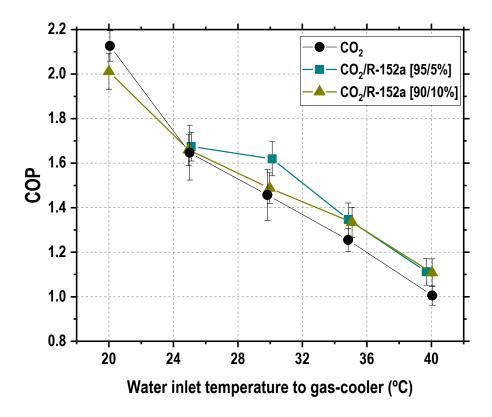
Figure 4. Evolution of the maximum COP for optimal conditions vs condenser/gas-cooler water inlet temperature for Base configuration.

3.1.2 Cooling capacity

Analysing the cooling capacity obtained for the use of the three tested fluids at optimal working conditions, it can be seen that the cooling capacity obtained with the use of pure CO_2 is higher than that obtained by using both the evaluated mixtures, due to the lower volumetric cooling capacity of the blends. As a matter of fact, the higher the mass proportion of R-152a, the lower cooling capacity is generated, as it can be seen in Figure 5. However, this slight reduction in cooling capacity reduction of the cooling capacity which can be offset thanks to a proper size design of the plant or even controlling the compressor's rotation speed depending on the needs.
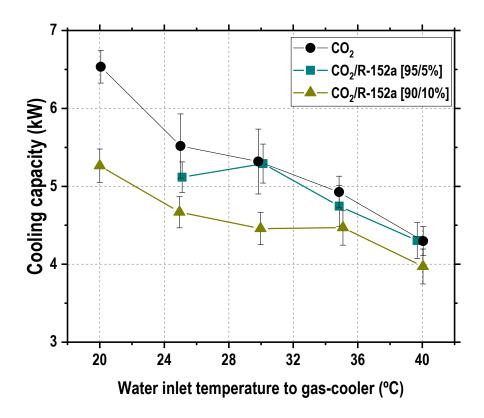
Figure 5. Evolution of the maximum cooling capacity for optimal conditions vs condenser/gas-cooler water inlet temperature for base configuration

3.1.3 Optimum working parameters

Gas-cooler pressure has a major effect on the performance of the plants and has to be optimized in CO_2 transcritical cycles. The use of a blend instead of pure CO_2 in the system changes the value of the optimum pressure, as shown in Figure 6. For all the three tested fluids the trend is towards a lower gas-cooler pressure when increasing the mass fraction of R-152a. This is a positive effect for the reliability of the system. It can be observed that the trend of the optimum gas-cooler pressure depending on the environment temperature is very linear, which makes it easy to control thanks to the expansion valve with a simple PID control.
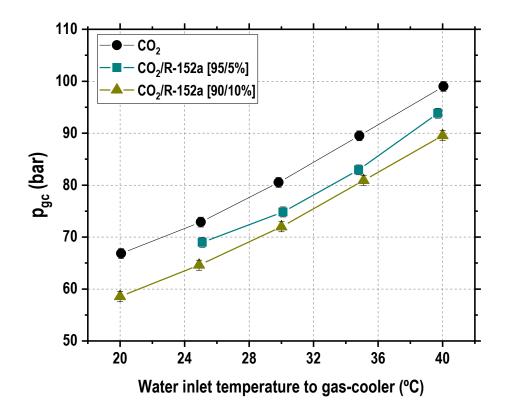
Figure 6. Optimum gas-cooler pressure vs condenser/gas-cooler water inlet temperature for base configuration.

Figure 7 represents the evolution of the compressor discharge temperature for the different conditions: using the tested blends instead of pure CO_2 increased the measured discharge temperature and this phenomenon was more significant at higher concentration of R-152a.
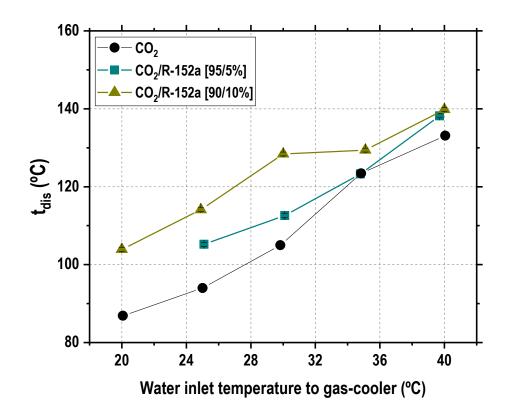
Figure 7. Compressor discharge temperature for optimal conditions vs condenser/gas-cooler water inlet temperature for base configuration.

3.2. IHX configuration

The cooling capacity of this configuration is calculated the same way as the base cycle configuration exposed in Eq. (1). The calculation of the COP and the heat balances in the gas-cooler/condenser and the evaporator are performed following Eqs. (4).

The difference between this cycle and the base cycle is the addition of an internal heat exchanger (IHX) that subcools the working fluid downstream the exit of the gas-cooler and heats up the fluid upstream the inlet of the compressor. Heat transfer analysis is performed in both currents flowing through the IHX as shown in Eq. (9) and Eq. (10) and the efficiency of the internal heat exchanger is calculated by Eq. (11).

$$\dot{Q}_{ihx} = \dot{m}_{ref} \cdot (h_{gc,out} - h_{ihx,h,out}) \tag{9}$$

$$\dot{Q}_{ihx,l} = \dot{m}_{ref} \cdot (h_{ihx,b,out} - h_{ihx,b,in}) \tag{10}$$

$$\varepsilon_{ihx} = \frac{t_{ihx,v,out} - t_{ihx,v,in}}{t_{ihx,l,in} - t_{ihx,v,in}} \cdot 100 \tag{11}$$

3.2.1 COP

Figure 8 shows the COP values obtained with the use of the tested fluids for different conditions of the secondary fluid at the inlet of the gas-cooler/condenser. It can be observed that the best energy performance is carried out using pure CO_2. The introduction of a second component in the mixture worsens significantly the COP of the system at

temperature below 30ºC, while above the mentioned temperature the COP obtained with the use of all three tested fluids are very similar. This is mostly due to the variations in the cooling capacity.
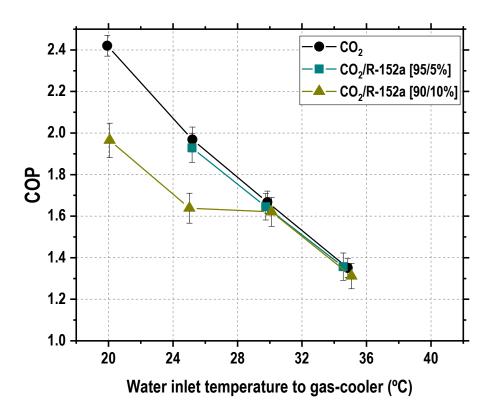
Figure 8. Maximum COP for optimal conditions vs. condenser/gas-cooler water inlet temperature for IHX configuration.

3.2.2 Cooling capacity

Cooling capacity for optimal conditions are displayed in Figure 9. It can be inferred that the introduction of R-152a as an additive in the pure CO_2 causes a reduction in the cooling capacity and this phenomenon is more significant as the mass composition of R-152a increases also due to the reduction in the VCC. The main conclusion extracted from these results is the decrease of cooling capacity of the cycle working with CO_2/R-152a mixtures in comparison with the $\dot{Q}_o$ obtained with the use of pure CO_2 for both architectures.

For the CO_2/R-152a composition [90/10%] at 25°C of heat rejection temperature, a sharp decrease in the cooling capacity is observed compared to one obtained with an inlet temperature of the secondary fluid at the condenser/gas-cooler of 30°C. The reason for this decline may be the change of operation conditions. At a heat rejection temperature of 25ºC the plant works under subcritical conditions, with a temperature approach to the hot sink of almost 4 K. When the plant is run with a heat rejection temperature of 30°C the approach is less than 1 K, due to the better heat transfer properties. Since the point at 25ºC is subcritical, the plant operates with the BP fully open. Forcing the condensing pressure could in this case improve the cooling capacity of the plant. As it can be seen in Figure 10, the enthalpy difference in the evaporator for 25ºC and 30ºC of the secondary fluid at the inlet of the condenser/gas-cooler is nearly the same while the mass flow circulating at 30ºC is higher, so the cooling capacity is also higher for this condition.
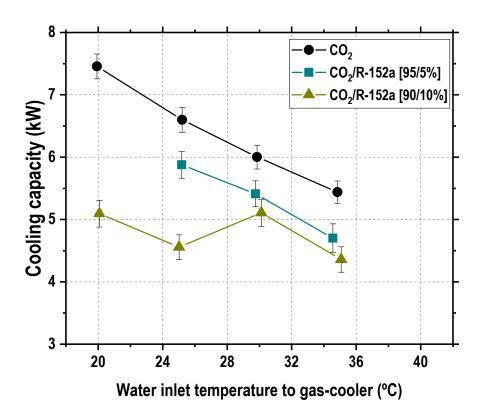
Figure 9. Cooling capacity for optimal conditions vs. condenser/gas-cooler water inlet temperature for IHX configuration.
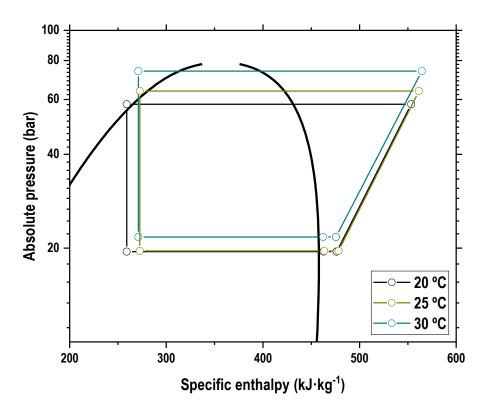
Figure 10. Ph diagram of CO_2/R-152a [90/10%] for IHX configuration at $t_{w,in}$=20, 25 and 30 ºC at optimum condition.

3.2.3 Optimum working parameters

Figure 11 presents the behaviour of the condenser/gas-cooler pressure and the compressor discharge temperature, at different conditions for the IHX cycle. As it can be observed, the behaviour and tendencies are similar to the ones observed in the base cycle i.e. using CO_2/R-152a mixtures as refrigerants instead of pure CO_2 cause reductions of the condenser/gas-cooler pressure and increments in the compressor discharge temperature. One significant difference is the generalised increase of the compressor discharge temperature in the cycle with IHX, due to the additional heat exchanger which leads to increased suction temperature. Because of this effect, tests at 40 °C could not be done, otherwise the discharge temperature would have exceeded the compressor limit.
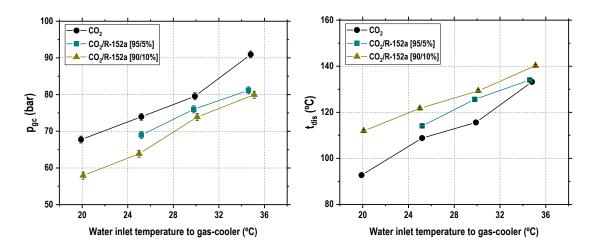
Figure 11. Optimum condenser/gas-cooler pressure and compressor discharge temperature vs water inlet temperature for IHX configuration.

The thermal effectiveness of the IHX (Eq. (11)) calculated for the tested conditions is between 35% and 45%. It seems that the addition of R-152a enhances slightly the thermal effectiveness of the heat exchanger, however the measurement uncertainty is too bit to draw a firm conclusion about this improvement. In the base cycle, when the mixtures were used as working fluids, subcooling is achieved in the condenser without modifying the working conditions of the compressor while using the IHX also increases the suction temperature, which penalizes cycle performance. The values of electrical power and compressor discharge temperature can be consulted in Table 4. As it can be seen in Table 5, the increment of the enthalpy difference due to the use of the IHX is higher when working with pure CO_2 and decreases with the addition of R-152a which makes that the use of the IHX is not so profitable when working with mixtures.

Table 5. Enthalpy difference due to the use of the IHX.

Figure 12 shows the IHX cycles at optimum conditions depicted in the (p-h) diagrams of the three tested fluids, for a fixed heat rejection temperature of 30ºC. With higher concentrations of R-152a in the working fluid, the optimal heat rejection pressure is lower and, at the same time, the critical pressure of the fluid, obtained by "*Refprop v.10*", is higher. These two phenomena caused by the use of blends make the cycle work in subcritical conditions.

CO₂

CO₂/R-152a [95/5%]

CO₂/R-152a [90/10%]
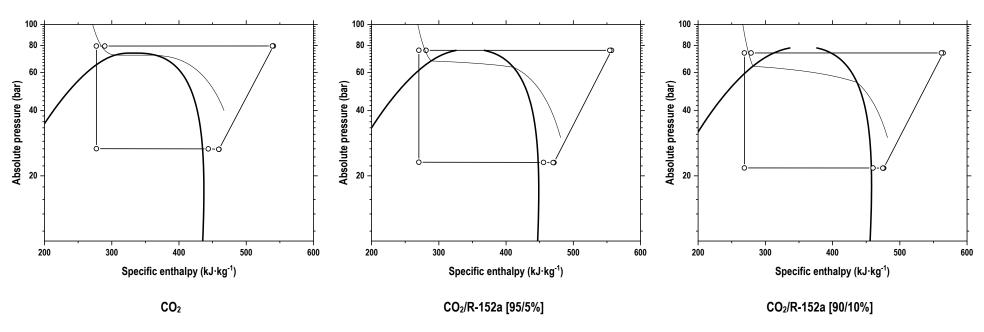
Figure 12. Ph diagram of CO_2 and mixtures for IHX configuration at $t_{w,in}$=30 ºC at optimum condition.

Lastly, one of the main differences between using IHX configuration or not do it rely on the superheating degree at the suction on the compressor. In this case, superheating is divided into two different superheating. The first one controlled by the electronic expansion valve has constant values that go between 4K and 6K of superheating at the exit of the evaporator. The remaining superheating degree is caused by the IHX; it has values between 10K and 15K depending on the conditions (bigger superheating at higher heat rejection temperatures). The detailed data is provided in Table 4.

3.3. Energy improvements

Table 6 contrasts the COP at best performing conditions obtained by the use of each fluid. It shows the COP increments or decrements as defined in the table for all three tested fluids and both base cycle and IHX cycle. It can be noted that at lower gas-cooler water inlet temperatures the use of pure CO_2 outperformed the use of CO_2/R-152a mixtures. On the contrary, at higher gas-cooler water inlet temperatures, using the mixtures allowed a slight improvement in the COP compared to that with the use of pure CO_2.

Figure 13 shows the COP increments obtained in the base cycle using mixtures referring to the use of pure CO_2. As it can be observed, for heat rejection temperature higher than 25 ºC, the mixtures always provide a COP improvement. This improvement is higher for the mixture CO_2/R-152a [95/5%] where the increments are 1.6% for 25.0 ºC, 11.2 for 30.0 ºC, 7.3% for 35.0 ºC and 10.6% for 40.0 ºC.
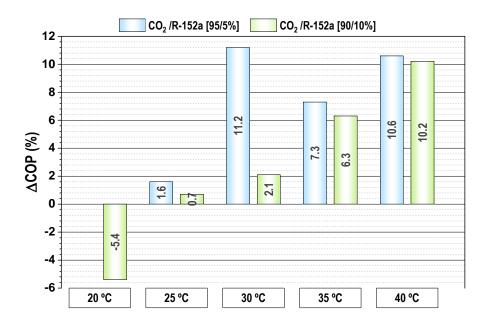
Figure 13. COP variations for base configuration.

Figure 14 depicts the COP variation accomplished in the IHX configuration. As it can be seen, the use of mixtures significantly decreases the COP of pure CO_2. With the blend CO_2/R-152a [95/5%] the reductions are lower than 2% but for the composition with 10% of R-152a, the COP decrements are important, reaching -18.6% at the lower temperature.
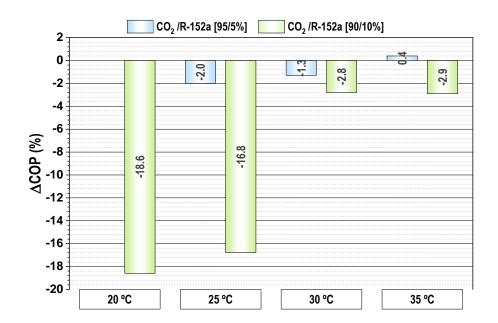
Figure 14. COP increments for IHX configuration

This work aims to enhance the COP of a base cycle without and with IHX by using mixtures. As it has been discussed, CO_2/R-152a produces COP increments for base cycle while it produces decrements when using IHX configuration.

When comparing all COP values, cycle with internal heat exchanger has higher COP values due to the additional component. The IHX is beneficial for the cycle and is well-designed, however, when using it in combination with CO_2/R-152a mixtures it does not work as good as it does with pure carbon dioxide.

4. Conclusions

This work presents experimental results and comparison of a CO_2 base refrigeration cycle with and without internal heat exchanger (IHX) working with CO_2/R-152a mixtures at 5% and 10% mass composition of R-152a as refrigerants. The experimentation is performed along heat rejection levels of 20ºC, 25ºC, 30ºC, 35ºC and 40ºC and at one inlet temperature in the evaporator of 2.5ºC, at steady-state conditions. The compressor run at nominal speed and the optimization parameter for both cycles was the gas-cooler pressure controlled with the Back-Pressure valve. All the obtained results have been validated by energy balances in the heat exchangers.

The experimental campaign has allowed to demonstrate the enhancement of COP in typical CO_2 cycles with the use of mixtures replacing pure CO_2. Using CO_2/R-152a blends instead of pure CO_2 as refrigerants in a base cycle improved the COP at high heat rejection temperatures. The use of CO_2/R-152a [90/10%] mixture provided COP improvements of 6.3% and 10.2% for $t_{w,in}$=35ºC and $t_{w,in}$=40ºC, respectively. Using CO_2/R-152a [95/5%] gave improvements of 7.3% and 10.6% for the same heat rejection temperatures and a maximum COP improvement of 11.2% for $t_{w,in}$=30ºC. On the other hand, for cycle with IHX, using the evaluated mixtures as working fluids instead of pure CO_2 was always detrimental for the energy efficiency, except for the case of the use of the blend CO_2/R-152a [95/5%] with $t_{w,in}$=35°C, which improved the COP by 0.4%.

The COP of the cycle is the main parameter studied, however, other parameters such as cooling capacity, heat rejection pressure or discharge temperature of the compressor have been considered as well. As a consequence of

the use of blends, some disadvantages were found: cooling capacity is reduced and the discharge temperature of the compressor is increased. However, the optimum heat rejection pressure is reduced, which is an advantage of using mixtures because it allows the cycle to work in subcritical conditions, where the control is easier, and it can allow to avoid using the liquid receiver.

The importance of this work relies on the COP enhancement of typical CO_2 cycles by using CO_2 based mixtures instead of pure CO_2 as working fluids. It is noted that COP improvements take place particularly at high heat rejection temperatures. Selection of the cycle configuration is also important as base cycle has significant improvements at high temperatures while cycle with IHX do not. COP obtained with base cycle with mixtures is almost equal to that of IHX cycle with pure CO_2 for high heat rejection temperatures which implies a reduction of the compressor discharge temperature and the non-existence of the additional heat exchanger (IHX), two mentionable feats due to CO_2/R-152a blends utilization. Some future research can be developed as for example determining experimentally the optimum composition of the mixture or testing other additives. Studying the mixture impact on more complex cycles such as the integrated mechanical subcooling can also be beneficial for the overall cycle behaviour.

Acknowledgements

References

Aprea, C., de Rossi, F., Mastrullo, R., 1997. The uncertainties in measuring vapour compression plant performances. Measurement 21, 65-70.

ATMOsphere, 2022. Natural Refrigerants: state of the industry. Commercial and industrial refrigeration in Europe.

Bell, I.H., Lemmon, E.W., 2016. Automatic Fitting of Binary Interaction Parameters for Multi-fluid Helmholtz-Energy-Explicit Mixture Models. Journal of Chemical & Engineering Data 61, 3752-3760.

Bush, J., Beshr, M., Aute, V., Radermacher, R., 2017. Experimental evaluation of transcritical CO2 refrigeration with mechanical subcooling. Science and Technology for the Built Environment, 1-13.

Catalán-Gil, J., Llopis, R., Sánchez, D., Nebot-Andrés, L., Cabello, R., 2019. Energy analysis of dedicated and integrated mechanical subcooled CO2 boosters for supermarket applications. International Journal of Refrigeration 101, 11-23.

European Commission, 2014. Regulation (EU) No 517/2014 of the European Parliament and of the Council of 16 April 2014 on fluorinated greenhouse gases and repealing Regulation (EC) No 842/2006.

European Comission, 2023. Proposal for a Regulation of the European Parliament and of the Council on fluorinated greenhouse gases, amending Directive (EU) 2019/1937 and repealing Regulation (EU) No 517/2014, in: Comission, E. (Ed.).

Gullo, P., Hafner, A., Banasiak, K., 2018. Transcritical R744 refrigeration systems for supermarket applications: Current status and future perspectives. International Journal of Refrigeration 93, 269-310.

Karampour, M., Sawalha, S., 2018. State-of-the-art integrated CO_2 refrigeration system for supermarkets: A comparative analysis. International Journal of Refrigeration 86, 239-257.

Kumar, K., Kumar, P., 2019. Analysis of Propane + CO_2 mixture as a working fluid in a vapor compression refrigeration system., 8th Conference on Ammonia and CO_2 Refrigeration Technology. Proceedings: Orhid, North Macedonia, , 2019.

Lata, M., Gupta, D.K., 2020. Performance evaluation and comparative analysis of trans-critical CO_2 booster refrigeration systems with modified evaporative cooled gas cooler for supermarket application in Indian context. International Journal of Refrigeration 120, 248-259.

Lemmon E. W., I.H., B., L., H.M., O., M.M., 2018. NIST Standard Reference Database 23: Reference Fluid Thermodynamic and Transport Properties-REFPROP, Version 10.0, National Institute of Standards and Technology.

Martínez-Ángeles, M., Sicco, E., Toffoletti, G., Nebot-Andrés, L., Sánchez, D., Cabello, R., Cortella, G., Llopis, R., 2023. Evaluation of CO_2-doped blends in single-stage with IHX and parallel compression refrigeration architectures: International Journal of Refrigeration. International Journal of Refrigeration, 151, 50-62. https://doi.org/10.1016/j.ijrefrig.2023.03.009

Moffat, R.J., 1985. Using Uncertainty Analysis in the Planning of an Experiment. Journal of Fluids Engineering 107, 173-178.

Nebot-Andrés, L., Calleja-Anta, D., Sánchez, D., Cabello, R., Llopis, R., 2021a. Experimental assessment of dedicated and integrated mechanical subcooling systems vs parallel compression in transcritical CO_2 refrigeration plants. Energy Conversion and Management, 115051.

Nebot-Andrés, L., Calleja-Anta, D., Sánchez, D., Cabello, R., Llopis, R., 2022. Experimental assessment of dedicated and integrated mechanical subcooling systems vs parallel compression in transcritical CO_2 refrigeration plants. Energy Conversion and Management 252, 115051.

Nebot-Andrés, L., Sánchez, D., Calleja-Anta, D., Cabello, R., Llopis, R., 2021b. Experimental determination of the optimum intermediate and gas-cooler pressures of a commercial transcritical CO_2 refrigeration plant with parallel compression. Applied Thermal Engineering, 116671.

Purohit, N., Sharma, V., Sawalha, S., Fricke, B., Llopis, R., Dasgupta, M.S., 2018. Integrated supermarket refrigeration for very high ambient temperature. Energy 165, 572-590.

Sánchez, D., Cabello, R., Llopis, R., Catalán, J., Nebot, L., Calleja, D., Gil, E., 2019. Energy improvements in a stand-alone transcritical refrigeration system using a low-GWP mixture of CO_2/R1270, Refrigeration Science and Technology, pp. 2633-2640.

Sánchez D., Calleja-Anta, D., Nebot-Andrés, L., Catalán-Gil, J., Llopis. R., Cabello, R., 2020. Experimental analysis of alternative blends of refrigerants for CO_2 transcritical refrigeration., VIII Ibero-american congress on refrigeration sciences and technology, CYTEF 2020, Public Universtity of Navarra, Spain.

Sánchez, D., Vidan-Falomir, F., Larrondo-Sancho, R., Llopis, R., Cabello, R., 2023a. Alternative Co2-Based Blends for Transcritical Refrigeration Systems. International Journal of Refrigeration.

Sánchez, D., Vidan-Falomir, F., Nebot-Andrés, L., Llopis, R., Cabello, R., 2023b. Alternative blends of CO_2 for transcritical refrigeration systems. Experimental approach and energy analysis. Energy Conversion and Management 279.

Söylemez, E., Widell, K.N., Gabrielii, C.H., Ladam, Y., Lund, T., Hafner, A., 2022. Overview of the development and status of carbon dioxide (R-744) refrigeration systems onboard fishing vessels. International Journal of Refrigeration 140, 198-212.

Tobaly P., Terrier M. F., Bouteiller P., 2018. CO_2 + propane mixture as working fluid for refrigeration in hot climates. Experimental results of energy efficiency tests., 13th IIR Gustav Lorentzen Conference on Natural Refrigerants (GL2018). Proceedings. Valencia, Spain.

Vaccaro, G., Milazzo, A., Talluri, L., 2022. Thermodynamic assessment of trans-critical refrigeration systems utilizing CO_2-based mixtures. International Journal of Refrigeration.

Xie, J., Wang, J., Lyu, Y., Wang, D., Peng, X., Liu, H., Xiang, S., 2022. Numerical investigation on thermodynamic performance of CO_2-based mixed refrigerants applied in transcritical system. Journal of Thermal Analysis and Calorimetry 147, 6883-6892.

Yu, B., Wang, D., Liu, C., Jiang, F., Shi, J., Chen, J., 2018. Performance improvements evaluation of an automobile air conditioning system using CO_2-propane mixture as a refrigerant. International Journal of Refrigeration 88, 172-181.

Zhao, Z., Luo, J., Song, Q., Yang, K., Wang, Q., Chen, G., 2022. Theoretical investigation and comparative analysis of the Linde-Hampson refrigeration system using eco-friendly zeotropic refrigerants based on R744/R1234ze(Z) for freezing process applications. International Journal of Refrigeration.

Appendix 1. Uncertainties calculation

To evaluate the measurement uncertainties of $\dot{Q}_o$ and COP, the method proposed by (Moffat, 1985) and extended by (Aprea et al., 1997) was used. The previous mentioned method was broadened in this work to include the uncertainty of the refrigerant composition.

Mass composition error

The mass composition of the components of a mixture $[Z_1, Z_2]$ are expressed by:

$$Z_1 = \frac{M_1}{M_1 + M_2} \tag{A. 1}$$

$$Z_2 = \frac{M_2}{M_1 + M_2} \tag{A. 2}$$

The uncertainty of the mass composition of the first component is:

$$I_{Z_1} = \sqrt{\left(\frac{\delta Z_1}{\delta M_1} \cdot \varepsilon_M\right)^2 + \left(\frac{\delta Z_1}{\delta M_2} \cdot \varepsilon_M\right)^2} \tag{A. 3}$$

$$I_{Z_1} = \sqrt{\left(\frac{M_2}{(M_1 + M_2)^2} \cdot \varepsilon_M\right)^2 + \left(\frac{M_1}{(M_1 + M_2)^2} \cdot \varepsilon_M\right)^2} \tag{A. 4}$$

Thus, the value of the mass composition of the refrigerant mixture is:

$$Z + I_Z = [Z_1 + I_{Z_1}; 1 - Z_1 - I_{Z_1}] \quad \text{and}$$
$$Z - I_Z = [Z_1 - I_{Z_1}; 1 - Z_1 + I_{Z_1}] \tag{A. 5}$$

Enthalpy measurement error

From the experimental measurements (p and t) and using Refprop v.10 the specific enthalpy values are calculated. These values are subjected to an uncertainty derived by the accuracies (ε) of temperature and pressure measurement devices, as well as, to the uncertainty of the refrigerant composition (Z).

The uncertainty of the specific enthalpy is calculated as:

- For enthalpies calculated through p measurement (for saturated vapour $x_v = 1$):

$$h_o = f(p, x_v, Z) \tag{A. 6}$$

$$I_h = \sqrt{I_p + I_Z} \tag{A. 7}$$

$$I_p = \frac{|h_{p+} - h_o| + |h_{p-} - h_o|}{2} = \frac{|h(p + \varepsilon_p, x_v, Z) - h_o| + |h(p - \varepsilon_p, x_v, Z) - h_o|}{2} \tag{A. 8}$$

$$I_Z = \frac{|h_{Z+} - h_o| + |h_{Z-} - h_o|}{2} = \frac{|h(p, x_v, Z + I_Z) - h_o| + |h(p, x_v, Z - I_Z) - h_o|}{2} \tag{A. 9}$$

Thus, the value of the enthalpy is expressed by:

$$h = h_o \pm I_h \tag{A. 10}$$

- For enthalpies calculated through p and t measurements:

$$h_o = f(p, t, Z) \tag{A. 11}$$

$$I_h = \sqrt{I_p{}^2 + I_t{}^2 + I_Z{}^2} \tag{A. 12}$$

$$I_p = \frac{|h_{p+} - h_o| + |h_{p-} - h_o|}{2} = \frac{|h(p + \varepsilon_p, t, Z) - h_o| + |h(p - \varepsilon_p, t, Z) - h_o|}{2} \tag{A. 13}$$

$$I_t = \frac{|h_{t+} - h_o| + |h_{t-} - h_o|}{2} = \frac{|h(p, t + \varepsilon_t, Z) - h_o| + |h(p, t - \varepsilon_t, Z) - h_o|}{2} \tag{A. 14}$$

$$I_Z = \frac{|h_{Z+} - h_o| + |h_{Z-} - h_o|}{2} = \frac{|h(p, t, Z + I_Z) - h_o| + |h(p, t, Z - I_Z) - h_o|}{2} \tag{A. 15}$$

Thus, the value of the enthalpy is expressed by:

$$h = h_o \pm I_h \tag{A. 16}$$

Cooling capacity uncertainty

Cooling capacity is computed as product of the refrigerant mass flow rate and the enthalpy difference in the evaporator, where isenthalpic expansion is assumed ($h_{o,in} = h_{bp,in}$), as detailed by:

$$\dot{Q}_o = \dot{m}_{ref} \cdot (h_{o,out} - h_{bp,in}) \tag{A. 17}$$

Its uncertainty is evaluated with:

$$I_{\dot{Q}_o} = \sqrt{\left(\frac{\delta \dot{Q}_o}{\delta \dot{m}_{ref}} \cdot \varepsilon_{\dot{m}}\right)^2 + \left(\frac{\delta \dot{Q}_o}{\delta h_{o,out}} \cdot I_{h_{o,out}}\right)^2 + \left(\frac{\delta \dot{Q}_o}{\delta h_{bp,in}} \cdot I_{h_{bp,in}}\right)^2} \tag{A. 18}$$

$$I_{\dot{Q}_o} = \sqrt{\left((h_{o,out} - h_{bp,in}) \cdot \varepsilon_{\dot{m}}\right)^2 + \left(\dot{m}_{ref} \cdot I_{h_{o,out}}\right)^2 + \left(\dot{m}_{ref} \cdot I_{h_{bp,in}}\right)^2} \tag{A. 19}$$

Thus, the value of cooling capacity is expressed by:

$$\dot{Q}_o = \dot{Q}_o \pm I_{\dot{Q}_o} \tag{A. 20}$$

COP uncertainty

COP is calculated as quotient of the cooling capacity and the measurement of the compressor power consumption,

$$COP = \frac{\dot{Q}_o}{P_C} \tag{A. 21}$$

Its uncertainty is evaluated with:

$$I_{COP} = \sqrt{\left(\frac{\delta COP}{\delta \dot{Q}_o} \cdot I_{\dot{Q}_o}\right)^2 + \left(\frac{\delta COP}{\delta P_C} \cdot \varepsilon_{P_C}\right)^2} \tag{A. 22}$$

$$I_{COP} = \sqrt{\left(\frac{1}{P_C} \cdot I_{\dot{Q}_o}\right)^2 + \left(\frac{-\dot{Q}_o}{P_C{}^2} \cdot \varepsilon_{P_C}\right)^2}$$

(A. 23)

The COP value is expressed as:

$$COP = COP \pm I_{COP}$$

(A. 24)

Table 1. Calibration range and measurement error of instrumentation

Measured variable	Device	Range	Calibrated error
Temperature	T-type thermocouple	-40.0 to 145.0 ºC	±0.5 K
High pressure	Pressure gauge	0.0 to 160.0 bar	± 0.96 bar
Medium pressure	Pressure gauge	0.0 to 100.0 bar	± 0.6 bar
Low pressure	Pressure gauge	0.0 to 60.0 bar	± 0.36 bar
Refrigerant mass flow rate	Coriolis	0.0 to 0.5 kg·s^{-1}	± 0.1% of reading
Evaporator glycol mass flow rate	Coriolis	0.0 to 13.88 kg·s^{-1}	± 0.1% of reading
Gas-cooler water volume flow rate	Magnetic flow meter	0.0 to 5.0 m^3·h^{-1}	± 0.3% of reading
Power consumption	Digital wattmeter	0.0 to 5.0 kW	± 0.5% of reading

Table 2. Thermophysical properties evaluated with Refprop v.10

Fluid	t_C (ºC)	p_C (bar)	p (t=-10ºC, x_v=0.5)	$\lambda_{(-10ºC)}$* (kJ·kg⁻¹)	$\nu_{v\,(-10ºC)}$ (m³·kg⁻¹)	$glide_{(-10ºC)}$* (K)	p (t=30ºC, x_v=0.5)	$\lambda_{(30ºC)}$* (kJ·kg⁻¹)	$glide_{(30ºC)}$* (K)
CO_2	30.98	73.77	26.49	258.6	0.0140	0	72.14	60.6	0
R-152a	113.26	45.17	1.81	317.0	0.1709	0	6.90	273.2	0
CO_2/R-152a [95/5 %]	36.58	76.93	24.65	272.6	0.0195	7.1	66.58	119.7	2.7
CO_2/R-152a [90/10 %]	41.58	78.82	22.84	284.6	0.0261	13.3	61.45	151.8	6.6

* Properties evaluated for pressure corresponding to the temperature and vapour title of 50%

Table 3. Test and optimum conditions and energy parameters of Base configuration

	Test conditions				Optimum cycle conditions						Energy parameters and uncertainty								
	$t_{w,in}$ (ºC)	$V_{w,in}$ (m³·h⁻¹)	$t_{g,in}$ (ºC)	$V_{g,in}$ (m³·h⁻¹)	p_h (bar)	p_{ves} (bar)	p_o (bar)	Δt_{gc} (K)	SH (K)	t_{dis} (ºC)	$\dot{m}_{ref}$ (kg·s⁻¹)	$\dot{Q}_O$ (kW)	$\dot{Q}_{O,sf}$ (kW)	P_C (kW)	$\dot{Q}_{gc}$ (kW)	$\dot{Q}_{gc,sf}$ (kW)	COP (-)	I_{Qo} (%)	I_{COP} (%)
CO₂	20.1	1.17	2.55	0.69	66.83	63.08	26.05	5.8	5.7	86.9	0.0392	6.53	6.46	3.07	9.23	9.25	2.13	3.2	3.2
	25.0	1.17	2.49	0.70	72.88	67.03	27.50	4.3	4.8	94.0	0.0398	5.52	5.51	3.35	8.96	8.77	1.65	7.5	7.5
	29.8	1.17	2.52	0.70	80.51	70.24	27.80	2.5	6.4	105.0	0.0391	5.32	5.31	3.65	8.86	8.52	1.46	7.8	7.8
	34.8	1.17	2.52	0.70	89.49	62.48	26.66	0.1	7.1	123.4	0.0343	4.93	4.85	3.93	8.35	8.50	1.25	4.1	4.2
	40.0	1.17	2.49	0.70	99.00	63.47	27.14	0.3	7.4	133.1	0.0332	4.30	4.18	4.27	7.93	8.09	1.01	4.3	4.3
CO₂/R-152a [95/5%]	25.1	1.17	2.52	0.70	68.99	65.24	22.74	1.9	6.2	105.2	0.0313	5.12	5.02	3.06	8.23	8.07	1.67	3.4	3.4
	30.1	1.17	2.53	0.70	74.83	71.96	23.23	1.3	6.2	112.6	0.0312	5.29	5.18	3.27	7.89	7.68	1.62	3.6	3.6
	34.8	1.17	2.49	0.70	82.94	80.65	23.65	0.3	6.3	123.3	0.0302	4.74	4.63	3.52	7.54	7.37	1.35	3.9	3.9
	39.7	1.18	2.54	0.70	93.83	91.68	24.13	0.2	6.2	138.2	0.0291	4.30	4.23	3.87	7.39	7.32	1.11	3.9	4.0
CO₂/R-152a [90/10%]	20.0	1.17	2.48	0.70	58.54	57.16	19.56	3.4	5.8	103.9	0.0266	5.26	5.19	2.62	7.49	7.44	2.01	4.0	4.0
	24.9	1.17	2.54	0.70	64.59	63.20	19.62	2.5	5.8	114.1	0.0256	4.67	4.62	2.81	7.11	7.08	1.66	4.2	4.2
	30.0	1.17	2.47	0.70	71.98	66.32	19.57	0.6	5.9	128.4	0.0240	4.46	4.32	3.00	6.77	6.75	1.49	4.3	4.3
	35.1	1.18	2.49	0.70	80.90	74.77	21.73	0.5	2.1	129.4	0.0270	4.47	4.41	3.35	7.17	6.97	1.33	4.0	4.0
	40.0	1.17	2.49	0.70	89.54	83.64	21.99	0.4	2.1	139.8	0.0261	3.97	3.95	3.58	6.85	6.52	1.11	4.2	4.3

Table 4. Test and optimum conditions and energy parameters of IHX configuration

	Test conditions				Optimum cycle conditions							Energy parameters and uncertainty											
	$t_{w,in}$ (ºC)	$V_{w,in}$ (m³·h⁻¹)	$t_{g,in}$ (ºC)	$V_{g,in}$ (m³·h⁻¹)	p_h (bar)	p_{ves} (bar)	p_o (bar)	Δt_{gc} (K)	SH_{EV} (K)	SH_{IHX} (K)	t_{dis} (ºC)	$\dot{m}_{ref}$ (kg·s⁻¹)	$\dot{Q}_O$ (kW)	$\dot{Q}_{O,sf}$ (kW)	P_C (kW)	$\dot{Q}_{gc}$ (kW)	$\dot{Q}_{gc,sf}$ (kW)	$\dot{Q}_{ihx}$ (kW)	$\dot{Q}_{ihx,l}$ (kW)	ε_{ihx} (%)	COP (-)	I_{Qo} (%)	I_{COP} (%)
CO₂	19.9	1.17	2.54	0.70	67.74	54.65	26.00	1.3		10.2	92.7	0.0378	7.46	7.49	3.08	9.99	10.43	0.499	0.523	39.4	2.42	2.9	2.9
	25.2	1.17	2.48	0.71	73.93	59.05	25.80	1.2	5.9	11.3	108.8	0.0353	6.50	6.60	3.35	9.25	9.12	0.498	0.512	36.0	1.94	3.0	3.0
	29.9	1.17	2.51	0.70	79.54	67.53	26.70	1.1	5.9	12.4	115.6	0.0356	5.93	6.00	3.60	8.88	8.71	0.502	0.575	35.4	1.65	3.2	3.2
	34.8	1.17	2.49	0.70	90.95	72.49	27.34	0.1	6.1	13.8	133.2	0.0338	5.39	5.44	4.03	8.66	8.63	0.496	0.607	35.9	1.34	3.3	3.3
CO₂/R-152a [95/5%]	25.2	1.17	2.56	0.70	69.00	59.21	22.71	1.6	6.2	11.7	114.1	0.0299	5.88	5.81	3.05	8.18	8.22	0.343	0.386	39.9	1.93	3.5	3.5
	29.8	1.17	2.51	0.70	75.98	62.89	23.12	0.6	6.2	11.5	125.6	0.0289	5.41	5.31	3.29	7.91	7.99	0.351	0.415	40.2	1.65	3.6	3.6
	34.6	1.17	2.50	0.70	81.17	73.68	23.71	0.3	6.2	15.6	134.0	0.0285	4.70	4.59	3.47	7.48	7.40	0.249	0.292	42.9	1.36	3.9	3.9
CO₂/R-152a [90/10%]	20.1	1.17	2.48	0.70	57.92	56.64	19.59	3.8	5.8	12.1	111.9	0.0255	5.09	5.07	2.59	7.39	7.23	0.091	0.260	43.4	1.97	4.1	4.1
	25.0	1.17	2.54	0.70	63.87	62.58	19.66	2.7	5.8	13.1	121.7	0.0248	4.56	4.52	2.78	7.06	6.86	0.053	0.303	44.0	1.64	4.3	4.3
	30.1	1.17	2.55	0.70	73.88	62.24	21.76	0.9	4.1	11.5	129.3	0.0267	5.11	4.99	3.15	7.56	7.79	0.250	0.351	39.8	1.62	3.9	3.9
	35.1	1.17	2.48	0.70	79.96	70.07	21.58	0.1	4.5	16.4	140.2	0.0251	4.36	4.32	3.32	6.98	6.74	0.150	0.443	45.4	1.31	4.2	4.2

Table 5. Enthalpy difference due to the use of the IHX.

$t_{w,in}$	Δh_0 (kJ·kg^{-1})					
20ºC	CO$_2$	8.02	CO$_2$/R-152a [95/5%]		CO$_2$/R-152a [90/10%]	6.86
25ºC		15.23		11.69		5.53
30ºC		13.42		11.77		11.73
35ºC		13.70		5.84		5.92

Table 6. All configurations and fluids comparison.

	BASE					IHX							
	CO$_2$	CO$_2$/R-152a [95/5%]		CO$_2$/R-152a [90/10%]		CO$_2$		CO$_2$/R-152a [95/5%]			CO$_2$/R-152a [90/10%]		
$t_{w,in}$ (°C)	$COP_{CO_2,Base}$	$COP_{mix,Base}$	$\frac{(COP_{mix,Base}-COP_{CO_2,Base})}{COP_{CO_2,Base}}$ (%)	$COP_{mix,Base}$	$\frac{(COP_{mix,Base}-COP_{CO_2,Base})}{COP_{CO_2,Base}}$ (%)	$COP_{CO_2,IHX}$	$\frac{(COP_{CO_2,IHX}-COP_{CO_2,Base})}{COP_{CO_2,Base}}$ (%)	$COP_{mix,IHX}$	$\frac{(COP_{mix,IHX}-COP_{CO_2,Base})}{COP_{CO_2,Base}}$ (%)	$\frac{(COP_{mix,IHX}-COP_{CO_2,IHX})}{COP_{CO_2,IHX}}$ (%)	$COP_{mix,IHX}$	$\frac{(COP_{mix,IHX}-COP_{CO_2,Base})}{COP_{CO_2,Base}}$ (%)	$\frac{(COP_{mix,IHX}-COP_{CO_2,IHX})}{COP_{CO_2,IHX}}$ (%)
20	2.13	-	-	2.01	-5.4	2.42	13.6	-	-	-	1.97	-7.6	-18.6
25	1.65	1.67	1.6	1.66	0.7	1.97	19.5	1.93	15.2	-2.0	1.64	-0.5	-16.8
30	1.46	1.62	11.2	1.49	2.1	1.67	14.4	1.65	1.6	-1.3	1.62	11.2	-2.8
35	1.25	1.35	7.3	1.33	6.3	1.35	7.7	1.36	0.8	0.4	1.31	4.5	-2.9
40	1.01	1.11	10.6	1.11	10.2	-	-	-	-	-	-	-	-